Infrared Physics & Technology 117 (2021) 103819

Contents lists available at ScienceDirect

Infrared Physics and Technology

journal homepage: www.elsevier.com/locate/infrared

Infrared star image denoising using regions with deep reinforcement learning

Zhenduo Zhang [a], Wenbo Zheng [a], Zhanjun Ma [a], Limei Yin [b,*], Ming Xie [a,*], Yuanhao Wu [b]

[a] *Navigation College, Dalian Maritime University, Dalian, China*
[b] *Changchun Institute of Optics, Fine Mechanics and Physics, Chinese Academy of Sciences, Changchun, China*

ARTICLE INFO

Keywords:
Star image
Image denoising
Geometric centroid method
Reinforcement learning
Maximum likelihood estimation
mixed Poisson–Gaussian likelihood

ABSTRACT

Efficient and accurate extraction and restoration of star targets in infrared star images with small number of frames is a growing need for optical adaptive image processing. Among the various noise in star images, mixed Poisson-Gaussian noise is difficult to be accurately suppressed due to its complicated distribution function. Aiming at obtaining the true value of star targets' signal intensity in infrared images, a novel star target extraction and denoising model called regions with deep reinforcement learning (RDRL) is designed and developed in this study. This fully-automatic model contains two modules: (1) star region extraction module (SREM) that generates star regions within the image through an iterative algorithm based on geometric centroid method (GCM); (2) denoising module that performs an iterative denoising process on the star regions based on deep reinforcement learning. The denoising algorithm is tested on infrared star images, and the experiment results indicate that the proposed RDRL denoising model is able to achieve more accurate restoration with a smaller number of calculations than existing star image denoising methods.

1. Introduction

Efficient and accurate extraction and restoration of star targets in astronomic images with small number of frames is a growing need for optical adaptive image processing [1,2]. Among the various noise in infrared star images (e.g., salt-and-pepper noise, strip noise, speckle noise, defective pixels, etc.) [3–7], mixed Poisson-Gaussian noise is intrinsically introduced by the optical responses of star sensor, and difficult to be accurately suppressed due to its complicated distribution function. Based on the fact that star sensors' measurements for all pixels are independent, Chouzenoux et al. developed a likelihood function for N frames of infrared star images with $M \times M$ pixels as Eq. (1) [8]:

$$p(zq|bq) = \prod_{q=1}^{N}\prod_{i=1}^{M^2}(\sum_{j=1}^{+\infty}\frac{e^{-[bq]_i}[bq]_i^j}{j!}\ \frac{e^{-\frac{1}{\sigma^2}([zq]_i-j)^2}}{\sqrt{2\pi\sigma^2}}) \tag{1}$$

where p is the probability of receiving the N observations, z_q is the noise image, b_q is the ground truth, σ is the variance of Gaussian distribution, subscript i is an index of pixels, q is an index of observations, and j is an index of the possible observations of the gray value in each pixel.

With the noise distribution function, the denoising problem could be solved through maximum likelihood estimation (MLE) method, which solves for the image that is most likely to produce the given observations. In this case, MLE method is intended to find a restore image b_0 that returns the highest value of the likelihood function as shown in Eq. (1). MLE method has been widely applied in astronomic image restoration [9–12]. Li et al. developed a multi-frame adaptive optical image denoising algorithm based on the distribution function of Poisson noise [12]. However, mixed Poisson-Gaussian noise has a much more complicated distribution function (Eq. (1)) and is difficult to be directly suppressed using MLE method. In order to solve this problem, Marnissi et al. further optimized the mixed Poisson-Gaussian likelihood function as Eq. (2) using generalized Anscombe transformation (GAT) approximation [13]:

$$p(zq|bq) = \prod_{i=1}^{M^2}\frac{1}{\sqrt{2\pi}}exp(-\frac{1}{2}(zq-2\sqrt{[bq]_i+\frac{3}{8}+\sigma^2})^2) \tag{2}$$

As indicated in Eq. (2), GAT method transforms the mixed Poisson-Gaussian function as a simplified Gaussian-like function, which can be solved using MLE method much more easily. However, GAT method inevitably introduces errors during the approximation [14]. Thus, restoration results from GAT method still have the potential to be further

* Corresponding authors.
E-mail addresses: yinlimei302@163.com (L. Yin), mingxie@dlmu.edu.cn (M. Xie).

https://doi.org/10.1016/j.infrared.2021.103819
Received 6 May 2021; Received in revised form 24 June 2021; Accepted 25 June 2021
Available online 29 June 2021

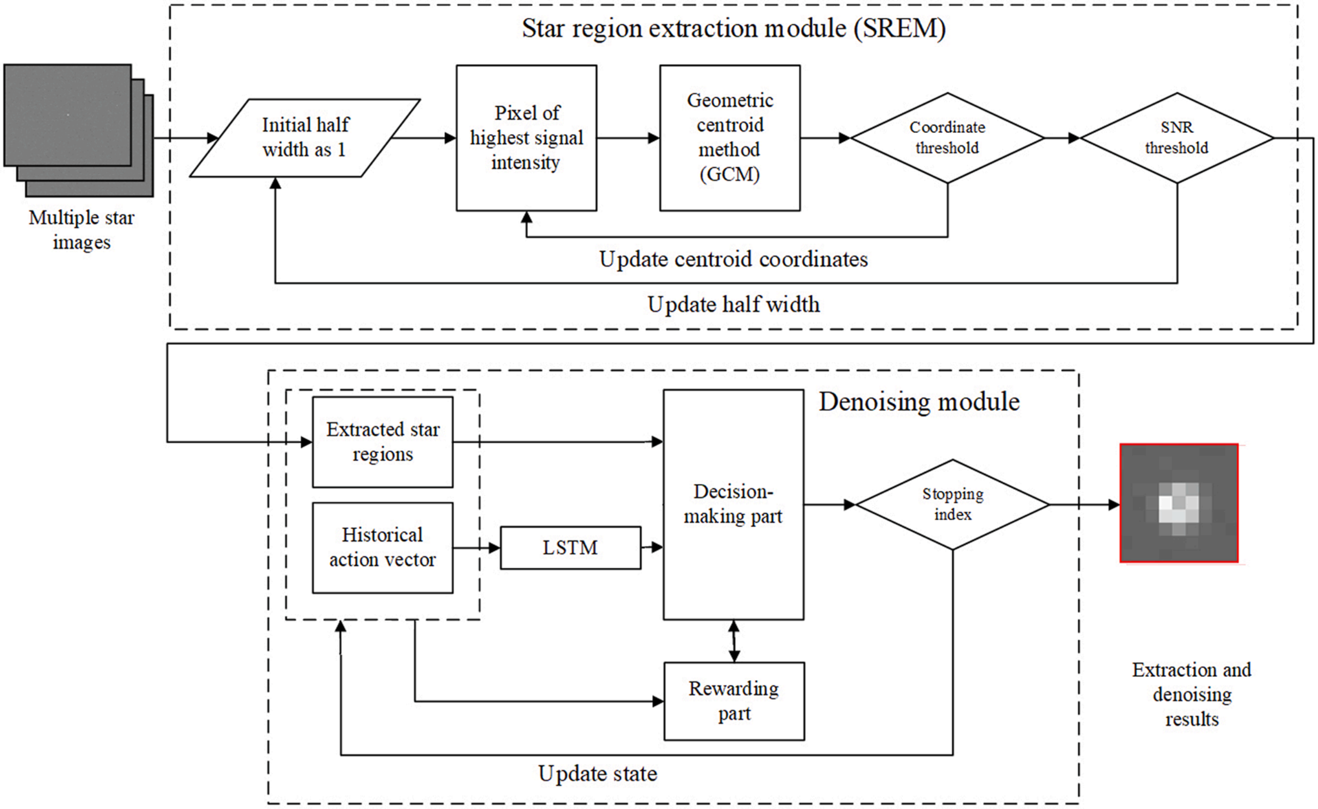

Fig. 1. Workflow of the proposed regions with deep reinforcement learning (RDRL) infrared star image denoising model.

improved.

The fast development of machine learning algorithm in the last decade opens up a new path for image processing [15]. Researchers has developed various models based on convolutional neural network (CNN) for image denoising [16–19] and deblurring [20–22]. Among the various advanced machine learning method, reinforcement learning (RL) is a classical algorithm that also received fast development. RL algorithms iteratively train an agent through its actions and evaluate how these actions change the environment. A reward function is usually defined in an RL model. The agent receives "rewards" or "punishments" based on the reward function, and aims to achieve higher rewards through continuous trials [23,24]. Built on this theoretical basis, Yu et al. developed a toolbox of image processing, and designed an RL-based image restoration algorithm by using the denoising tools in the toolbox [25]. In the field of star image denoising, Xie et al. developed a multi-frame star image denoising algorithm based on reinforcement learn (RL) and achieves more accurate restoration than traditional methods [26]. However, this algorithm involves a large amount of calculations, and could be time-consuming.

Considering the limitations in the previous studies on star image denoising, a regions with deep reinforcement learning (RDRL) algorithm that aims at the extraction of the true value of star targets' signal intensity in infrared image is designed and developed in this study. Infrared star images are collected and used for model training and testing. By applying RL-based denoising algorithm in extracted regions of star target, the proposed algorithm is expected to accurately and efficiently suppress the mixed Poisson-Gaussian noise in infrared star images.

2. Methodology

2.1. Equipment details and data acquisition

Infrared star images are collected and used to train and test RDRL model. The star sensor used in this study is a mercury cadmium telluride (MCT) camera of infrared focal plane array integrated with rotary Stirling cryocooler. The angular resolution for single pixel of the MCT camera is 4.7″, and the imaging spectral range of the camera is from 3.7 μm ~ 4.8 μm. The diameter of the telescope of the camera is 680 mm, the f-number is 2, and the field of view is 0.5°. The size of target surface is 320 × 256 and that of sensing unit is 30 μm × 30 μm. The outputs of the camera are 16-bits grayscale images, of which the gray values indicate the signal intensity.

The data acquisition experiment is conducted in northeast China on the ground under cloudless weather condition. The star target observed in the experiment is Alpha Tau (star number: HD29139), of which the apparent magnitude is 0.85. The camera is placed statically on the ground, and 2000 images are collected for the star target.

2.2. Data processing

The output infrared images from MCT camera need to be pre-processed in order to calibrate the optical responses between different sensing unit. Based on the two-point correlation method of black body and sky background, the calibration function of sensing units can be given as Eq. (3):

$$yij = Gijxij + Qij \tag{3}$$

where G_{ij} and Q_{ij} are the weight and bias factors of calibration; x and y are the outputs in each sensing unit before and after the calibration; i and j indicate the index of pixels in output images.

The weight factor of calibration G_{ij} is:

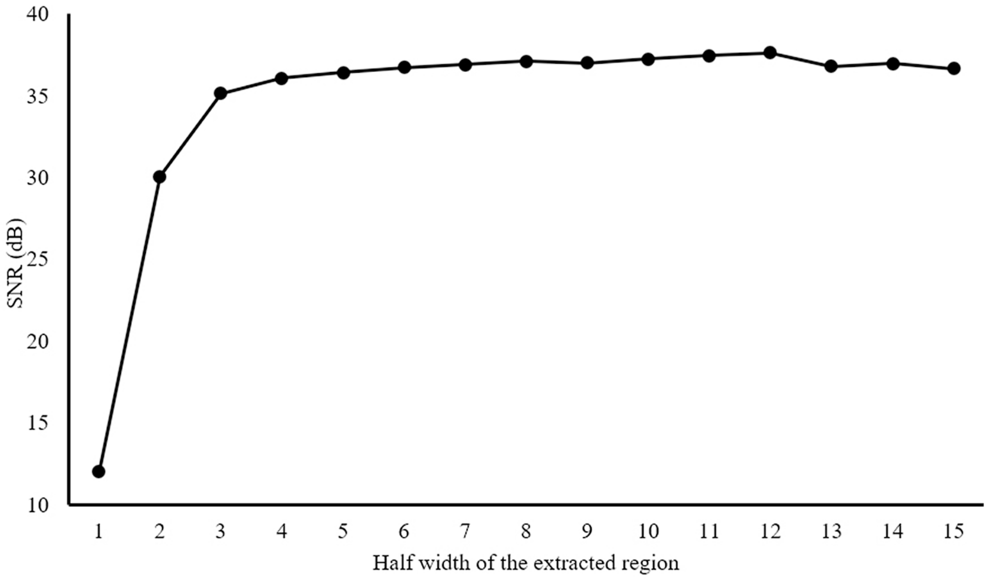

Fig. 2. Signal-to-Noise ratio (SNR) of star regions extracted using different half width.

$$Gij = \frac{V2 - V1}{xij(T2) - xij(T1)} \tag{4}$$

where T_1 and T_2 are the lowest and highest temperature of the black body for calibration; $x_{ij}(T_1)$ and $x_{ij}(T_2)$ are the outputs of sensing unit under temperature T_1 and T_2; V_1 and V_2 are the average outputs of all sensing units under temperature T_1 and T_2. Specifically, V_1 and V_2 are:

$$V1 = \frac{\sum_{i=1}^{M}\sum_{j=1}^{N} xij(T1)}{MN} \tag{5}$$

$$V2 = \frac{\sum_{i=1}^{M}\sum_{j=1}^{N} xij(T2)}{MN} \tag{6}$$

where M and N are the number of sensing units in each column and row.

The bias factor of calibration Q_{ij} is:

$$Qij = V3 - Gijxij(Tatmosphere) \tag{7}$$

where $T_{atmosphere}$ is the temperature of sky background, $x_{ji}(T_{atmosphere})$ is the output of sensing unit under $T_{atmosphere}$; V_3 is the average output of all sensing units under temperature $T_{atmosphere}$. Specifically, V_3 is:

$$V3 = \frac{\sum_{i=1}^{M}\sum_{j=1}^{N} xij(Tatmosphere)}{MN} \tag{8}$$

2.3. Regions with deep reinforcement learning (RDRL) algorithm

Different from general image denoising problem that aims at visually restoring the image, the goal of star image denoising is to find the signal intensity (indicated by gray value in the image) of star target as close to the ground truth as possible. Therefore, the denoising process in the background area with no star target, which usually occupies most of the area in a star image, is actually meaningless. Considering this characteristic of star image denoising problem, a two-steps star target extraction and denoising algorithm is designed in this study. Small square regions with star targets are extracted in the first module with an iterative region extraction algorithm, and then a denoising module is applied to the extracted star regions based on deep reinforcement learning. The overall workflow of proposed RDRL algorithm is shown as Fig. 1. The detailed steps in each of the two modules are discussed as follow.

2.3.1. Star region extraction module (SREM)

A star region extraction module (SREM) is designed to automatically detect and extract the regions with star targets in infrared star images. Since star targets usually spread into several pixels within the star images, the extracted regions are square regions of which the location and size are determined based on two parameters: region centre C (the central pixel of the square region) and half width d (number of pixels from the central pixel to the boundary pixel of the square region, excluding the central pixel). Thus, the extracted regions are squares that centre at C_{xy} and have side length of $2d + 1$. These two parameters are determined through an iterative calculation. In each step of the iteration, the region centres with a given half width is calculated though an internal-iteration based on geometric centroid method (GCM) [27]. GCM has been applied to locate and track star targets captured by star sensors [28–30]. The mathematic representation of GCM can be given as:

$$Cx, i+1 = \frac{\sum_{x=Cx,i-d}^{Cx,i+d} x\cdot DNx, y}{\sum_{x=Cx,i-d}^{Cx,i+d} DNx, y} \tag{9}$$

$$Cy, i+1 = \frac{\sum_{x=Cy,i-d}^{Cy,i+d} y\cdot DNx, y}{\sum_{y=Cy,i-d}^{Cy,i+d} DNx, y} \tag{10}$$

where × and y are the coordinates of pixels; DN_{xy} indicates the signal intensity of corresponding pixel; C_x and C_y are the coordinates of the region centre in each iteration; d is the half width of star region; i indicates the number of iterations. The initial position is set at the pixel with maximum gray value (signal intensity) in the star image. When the changes in region centre coordinates are smaller than 0.5 after numbers of iterations, GCM is considered to be converged, and the centre is determined as the coordinates in the last iteration.

In order to automatically find the appropriate half width of the star regions, SREM iterates from 1 to a maximum half width (MHW). In each step of this general iteration, Signal-to-Noise Ratio (SNR) of the extracted star region is calculated using Eq. (11).

$$SNR = \frac{\sum_{x=Cx-d,y=Cy-d}^{x=Cx+d,y=Cy+d} DNx, y - DNbg\cdot(2d+1)}{\sigma} \tag{11}$$

where σ is the variance of sky background, which is calculated using the boundary pixels of the star image. Because these pixels are far away from the star target, the Poisson noise (which positively correlates with signal intensity) within these pixels is ignorable and variance is expected to be contributed by Gaussian noise only. The SNR calculated under different half width is shown as Fig. 2.

As shown in Fig. 2, SNR has a positive correlation with half width in a limited range. Therefore, when SNR increases less than ten percent than that in the previous step, SREM is considered to be converged, and the final output region is determined by the combination of half width and region centre in the last iteration. The working flow of SREM is summarized in Algorithm 1.

Algorithm 1. Star Region Extraction Module (SREM)

```
Step 1: Determine the pixel with the largest gray value as the initial value: $C_{x,0}$,$C_{y,0}$;
    Calculation $\sigma$ using the boundary pixels.
Step 2: while d $<$ $MHW$ and $(SNR_d\text{-}SNR_{d\text{-}1})/SNR_{d\text{-}1} > 0.1$
while $|C_{x,i+1}\text{-}\ C_{x,0}| > 0.5$ or$|C_{y,i+1}\text{-}\ C_{y,0}| > 0.5$Process $C_{x,i}$,$C_{y,i}$ using geometrical
    centroid method (GCM, refer to Eq. (9) and (10) for details) and obtain $C_{x,i+1}$,$C_{y,i+1}$.
    end while
Calculate the Signal-to-Noise Ratio (SNR, refer to Eq. (11) for details) under each
    combination of center pixel ($C_{x,i}$,$C_{y,i}$) and half width $d$.end while
Step 3: Generate the star region based on ($C_{x,i}$,$C_{y,i}$) and $d$.
```

2.3.2. Denoising module for the extracted star regions

After the star regions are located in the infrared star images, denoising module is applied to the extracted star regions based on deep reinforcement learning. By applying the noise model as the reward function, the denoising agent would search for the restored image that returns highest rewarding, which equates to the image with highest possibility when using MLE method.

Deep Q-learning [31] is adopted to construct this RL model. Specifically speaking, this model consists of 4 parts:

(1) State part consists of a noise image, which is the output image in the previous iteration, and the historical action that is fed to a long short-term memory (LSTM) module in the next part. State part receives the star regions extracted by SREM, and uses the arithmetic mean of the star regions as the initial image. Combining with a zero vector, they form the initial state.

(2) Decision-making part takes a sequence of actions on the star image based on the state and reward function. Since infrared star images are grayscale images that illustrate signal intensity obtained by star sensor from a star, the choices of actions for any given pixel are either increasing/decreasing the gray value by w (which is a searching radius that gradually decreases to 1 as the iteration goes on), or stay at the same value. LSTM model is also included in the decision-making part to process the historical actions. LSTM is a special type of recurrent neural network (RNN) that includes an additional hidden state that decides to "remember" or "forget" previous input based on a gating function [32]. LSTM solves the problems of gradient vanishing or explosion in regular RNN by "forget" unnecessary inputs [33]. In the RDRL model proposed in this paper, the iterative actions performed by the decision-making part form a sequence dataset that can be effectively processed through LSTM. Therefore, LSTM provides additional information for current action selection, and enable the model to learn from previous actions.

(3) Rewarding part examines the input state and the action taken in the previous iteration, and then evaluates the action taken in the current iteration using a reward function. According to the mixed Poisson-Gaussian noise model in star image, the reward function applied in this study is defined as Eq. (12):

$$maxf(zq|b_q^{'})= log(\prod_{q=1}^{N}(p(zq|b_q^{'})) = \sum_{q=1}^{N}\sum_{i=1}^{M^2} log(\sum_{j=1}^{+\infty}\frac{e^{-[b_q^{'}]_i}[b_q^{'}]_i^j}{j!}\frac{e^{-\frac{1}{\sigma^2}([zq]_i-j)^2}}{\sqrt{2\pi\sigma^2}}) \tag{12}$$

Noting that there is an infinite term in the reward function. This term indicates the probability of receiving a given value in certain pixel. It decreases as the restored value gets further from the true value (it is not likely that the observed value is too far away from the true value). In practice, this term is dropped when it is smaller than 10^{-8} and has small influence on the rewards.

(4) Stopping part automatically stops the iteration when the number of iterations reaches the maximum number of iteration (MNI), or the decision-making part continuously chooses to stay at the same value (when the restored value reaches the ground truth, either increasing or decreasing the value would end up in a negative rewards).

The workflow of the denoising algorithm in the extracted star regions is summarized in Algorithm 2. There are several hyperparameters that need to be adjusted according to the quality of the noise images: (1) Initial searching radius (ISR) w_0, which is the searching radius w in the first iteration; (2) Stopping index (SI), which is defined as the number of times that decision-making part continuously chooses to stay at the same value; (3) MNI, which is also served as a threshold to stop the iteration together with SI.

Algorithm 2. Denoising module in the extracted star region

```
Step 1: Import extracted star regions from SREM. Obtain image size $M \times M$, and
    variance of Gaussian noise; Create initial input image as the arithmetic mean of $N$
    frames of noise image; define initial action vector $v_0$ as a zero vector; initialize
    stopping counter $c_s =$
Step 2: Define action table ($a_1 = +w$, $a_2 = \text{-}\ w$, $a_3 =$ no action); initialize action-value
    function $Q$ with random weight $\theta$
Step 3: for each of the $M \times M$ pixels in extracted star region: initialize sequence of
    state { $b_i$ }
while $i < MNI$ and $c_s < SI$:
Process $v_{i\text{-}1}$ through LSTM and obtain $v^{'}_{i\text{-}1}$
With probability $\varepsilon$ select $v_i$ = argmax $Q(b_{i\text{-}1}; v^{'}_{i\text{-}1}; \theta)$
Otherwise select a random action $v_i$ from action table
Execute action $v_i$, and then update environment $b_i = b_{i\text{-}1} + v_i$, and observed reward $r_i$
Update action-value function $Q$ with the observed ($b_i$; $v_i$; $r_i$)
After every 10 iterations $w \leftarrow$ rounding up ($w/2$)
if $a_3$ is chosen in this loop then: $c_s \leftarrow c_s + 1$
else: $c_s \leftarrow 0$
end if
end while
```

Compared with the RL-based denoising algorithm proposed by the Xie et al. in Ref. [26], there are two major improvements in the proposed algorithm: (1) the RL-based denoising module is only applied on the star regions extracted by SREM, thus the number of calculations and running time are expected to be significantly reduced; (2) the star regions and background regions are produced through SREM, which makes the overall denoising process fully-automatic.

2.4. Implementation details

Hyperparameters affect the accuracy of restoration results and the number of iterations (running time) in different way. Increasing SI could improve the accuracy of restored image in a limited extend, but is likely to cause more calculations. Larger ISR could reduce number of calculations, but may be unnecessary when the noise is rather small (especially when the noise is even smaller than ISR). Thus, these hyperparameters need to be calibrated through test running before denoising process. Since the star images used in this experiment are 16-bit grayscale images with relatively low noise, ISR is set at 10 and decrease by one half (rounding up) after every 10 iterations, SI is set at 4, and MNI is set at 500.

The proposed RDRL denoising model is built using Tensorflow backend [34] in Python 3.6 environment. The model is trained and

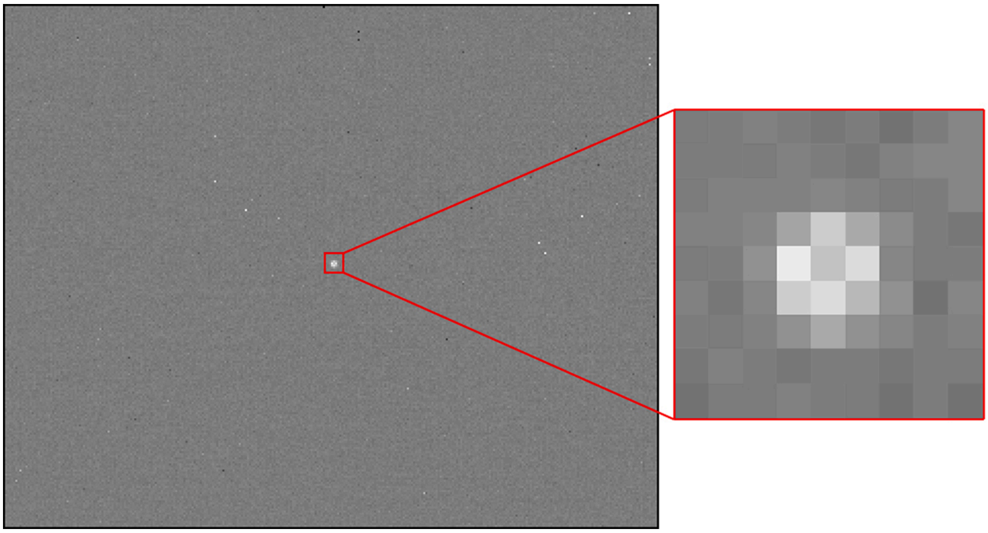

Fig. 3. An example of star image collected in the experiment. The extracted star region is shown in the red frame on the right.

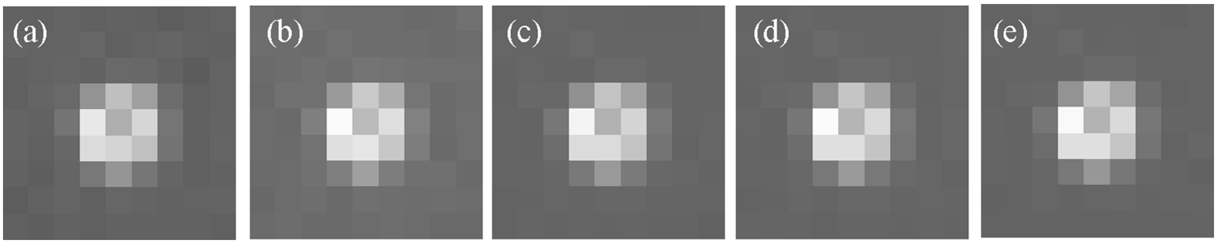

Fig. 4. Arithmetic mean of: (a) 10 frames; (b) 20 frames; (c) 50 frames; (d) 100 frames; (e) 500 frames of infrared star images.

Table 1
Signal-to-Noise Ratio (SNR) of the averaged images using 10, 20, 50, 100, 500 frames.

Number of frames	10	20	50	100	500
SNR (dB)	38.10	45.40	47.03	48.68	51.29

tested using 2.5 GHz Intel i5-7300HQ CPU with 8.0 GB of RAM running on a 64-bit Windows 10 operating system. For the denoising experiments in this study, the ε-greedy of Deep Q-learning [31] is set at 0.95. Adam [35] is used as the optimizer of the model, and hyperbolic tangent function is used as the gating function of LSTM.

3. Results

3.1. Star regions extraction results

As shown in Fig. 3, the star images collected by the star sensor are 16-bits grayscale images with the resolution at 320 × 256. The variance of Gaussian noise in the background of the star images is about 5.07, The extracted star regions are also shown in Fig. 3. The final half width of extracted star region is 4. Thus, the generated star regions are 9 × 9 squares. The star target visually locates in the centre of the star region as shown in Fig. 3. These results conform with the calculations using GCM by Tough [27].

3.2. Denoising results

The traditional method suppresses the noise in star image by taking arithmetic mean of multiple images. This method is tested and utilized as a scale to evaluate the performance of denoising algorithms. For the star target observed in this study, the average images of 10, 20, 50, 100, 500 frames of star target are shown as Fig. 4.

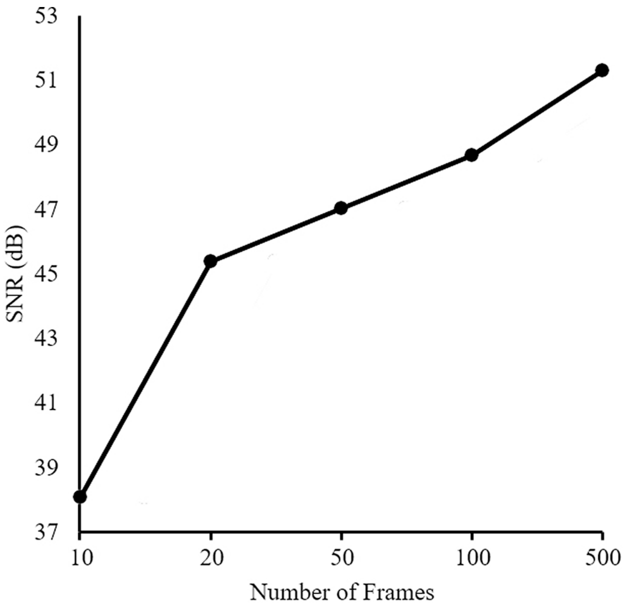

Fig. 5. SNR of the averaged images using different number of frames.

Because the true value is unknown for real star images, the accuracy is quantitatively evaluated through SNR, which is defined as Eq. (11). SNR of the averaged images using different number of frames are included in Table 1, According to the trend shown in Fig. 5, SNR increases as more frames of star images are used for averaging. This result

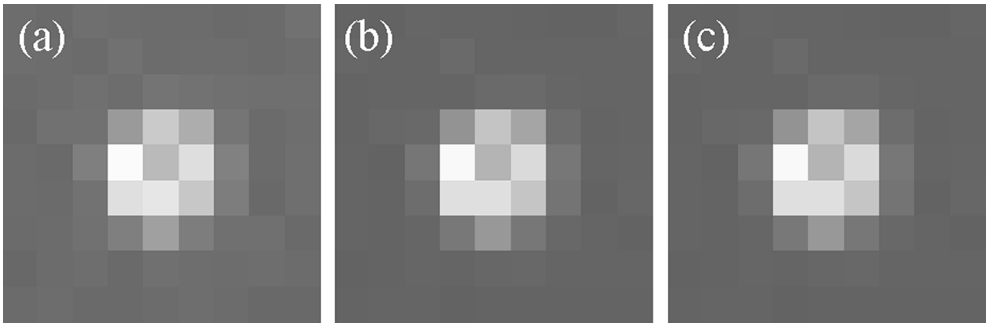

Fig. 6. Denoising results using 10 frames of star image and three different algorithms: (a) GATFP [36]; (b) RL-based [26]; (c) proposed method.

Table 2
SNR of the denoising results using 10 frames of noising images with three different methods.

	GATFP [36]	RL-based [26]	RDRL
SNR (dB)	46.26	48.23	48.47

Table 3
Number of parameters and calculations for two machine learning models.

	RL-based [26]	RDRL
Parameters ($\times10^4$)	11.0	3.26
Calculations ($\times10^7$)	22.6	8.32

validates the star image denoising method by averaging a large number of images.

The denoising experiments for the star target are conducted using 10 frames of star images and three different algorithms: RDRL proposed in this study, generalized Anscombe transformation approximation Fourier ptychographic (GATFP) method proposed by Zhang et al. [36] and RL-based method proposed by Xie et al. [26]. The performances of these algorithm are compared and evaluated with the scale of averaged star images. The denoising results within the extracted regions for the star images are shown in Fig. 6.

As shown in Fig. 6, it is difficult to recognize the differences between the restoration results using these three methods directly through human eyes. Therefore, the restoration results are quantitatively evaluated using SNR (Table 2). Compared with the SNR using arithmetic mean of multiple frames of star images (as shown in Table 1 and Fig. 5), the restoration results using 10 frames of noise images with the proposed method and the RL-based method [26] are close to the arithmetic mean of about 100 frames of noise images; while that with the GATFP method [36] is close to the arithmetic mean of about 50 frames of noise images.

The number of calculations is also recorded in Table 3. As we expected, the number of calculations using RDRL method proposed in this study is significantly smaller than that using the RL-based method proposed by Xie et al. [26].

4. Discussion

RDRL algorithm proposed in this study is able to extract the star region and suppress mixed Poisson-Gaussian noise fully-automatically. This model is compared with GATFP [36] and RL-based [26] method in terms of both accuracy and computational complexity. The denoising results of the two existing methods generally conformed with those presented in the previous studies. As indicated in Table 2, all the three methods are able to suppress the mixed Poisson-Gaussian noise better than taking the arithmetic mean of same number of noise images. There is no significant difference between the proposed method and the RL-based method [26] in term of restoration accuracy, and these two machine learning methods provides more accurate restoration than GATFP method [36]. This is probably because that the error introduced by the approximation of GAT is reduced by directly applying the distribution function of the noise as the reward function of the denoising algorithms. RDRL algorithm performs denoising results of similar accuracy as that using RL-based method because they share a similar rewarding mechanism in the rewarding part.

Furthermore, by comparing the computational complexity of RDRL and RL-based method [26], the number of calculations using RDRL method is significantly smaller than that using RL-based method. By adding SREM, a large number of calculations on the background area that is not meaningful to the extraction on the true value of star target are avoided in RDRL model. Therefore, the proposed method is able to achieve accurate restoration results with small number of calculations than the existing methods.

5. Conclusions and future studies

A fully-automatic and novel approach for infrared star image denoising is presented in this study. The proposed RDRL model consists of an SREM that automatically search for star regions, and a denoising module based on deep reinforcement learning. According to the experiments on infrared star images, the proposed RDRL model is able to achieve more accurate restoration than GATFP method, and using a smaller number of calculations than regular RL-based method.

The limitation of the proposed RDRL model is that SREM can only search for single star target that has highest signal intensity within one star image. Thus, this algorithm may not work properly when multiple star targets are needed to be extracted from a single image, or the target of interest is not the star that has the highest signal intensity within the star image. Another approach to further improve the performance of the model is to replace the pixel-by-pixel denoising procedure with CNN. By utilizing CNN's ability of recognizing spatial patterns, we envision a convolutional-RDRL denoising algorithm that can preserve the relations between pixels within star images, and thus further improve the restoration result.

Declaration of Competing Interest

The authors declare that they have no known competing financial interests or personal relationships that could have appeared to influence the work reported in this paper.

Acknowledgements

This research was funded in part by National Science Foundation of China [grant number 11703024], and in part by China Postdoctoral Science Foundation [grant number 2020 M670730]. The authors would also like to thank Kai Cao and Qinglai Yu from Dalian Maritime University for their help in preparing the training dataset.

Disclosures

The authors declare no conflicts of interest.

Data availability statement

The data involved in this study are not publicly available because they are obtained from a confidential project.

References:

[1] T. Sun, F. Xing, Z. You, Research on dynamic performance of star tracker, Instrumentation 2 (1) (2015) 17–26.

[2] C.R. McBryde, E.G. Lightsey, A star tracker design for CubeSats, IEEE Aerospace Conference (2012) 1–14, https://doi.org/10.1109/AERO.2012.6187242.

[3] H. Hwang, R.A. Haddad, Adaptive median filters: New algorithms and results, IEEE Trans. Image Process. 4 (4) (1995) 499–502, https://doi.org/10.1109/83.370679.

[4] B. Jin, N. Park, K.M. George, M. Choi, M.B. Yeary, Modeling and analysis of soft-test/repair for CCD-based digital X-ray systems, IEEE Trans. Instrum. Meas. 52 (6) (2003) 1713–11321, https://doi.org/10.1109/TIM.2003.818735.

[5] W. Wang, X. Wei, J. Lin, G. Wang, Noise suppression algorithm of short-wave infrared star image for daytime star sensor, Infrared Phys. Technol. 85 (2017) 382–394, https://doi.org/10.1016/j.infrared.2017.08.002.

[6] Z. Zhou, E.Y. Lam, C. Lee, Nonlocal means filtering based speckle removal utilizing the maximum a posteriori estimation and the total variation image prior, IEEE Access 7 (2019) 99231–99243, https://doi.org/10.1109/ACCESS.2019.2929364.

[7] P. Yugander, C.H. Tejaswini, J. Meenakshi, K. Samapath kumar, B.V.N. Suresh Varma, M. Jagannath, MR image enhancement using adaptive weighted mean filtering and homomorphic filtering, in: in *International Conference on Computational Intelligence and Data Science* (ICCIDS, 2019, pp. 667–685, https://doi.org/10.1016/j.procs.2020.03.334.

[8] E. Chouzenoux, A. Jezierska, J.C. Pesquet, H. Talbot, A convex approach for image restoration with exact Poisson-Gaussian likelihood, SIAM J. Imaging Sci. 8 (4) (2015) 2662–2682, https://doi.org/10.1137/15M1014395.

[9] J. Llacer and J. Nuiez, Iterative maximum-likelihood and Bayesian algorithms for image reconstruction in astronomy, in Restoration of Hubble Space Telescope Images, R. L. White and R. J. Allen, eds. (Space Telescope Science Institute, 1990), pp. 62-69.

[10] D.L. Snyder, A.M. Hammoud, R.L. White, Image recovery from data acquired with a charge-coupled-device camera, J. Opt. Soc. Am. A 10 (5) (1993) 1014–1023, https://doi.org/10.1364/JOSAA.10.001014.

[11] F. Benvenuto, A.L. Camera, C. Theys, A. Ferrari, H. Lanteri, M. Bertero, The study of an iterative method for the reconstruction of images corrupted by Poisson and Gaussian noise, Inverse Probl. 24 (3) (2008) 1–20, https://doi.org/10.1088/0266-5611/24/3/035016.

[12] D. Li, C. Sun, J. Yang, H. Liu, J. Peng, L. Zhang, Robust multi-frame adaptive optics image restoration algorithm using maximum likelihood estimation with Poisson statistics, Sensors 17 (4) (2017) 785, https://doi.org/10.3390/s17040785.

[13] Y. Marnissi, Y. Zheng, and J. C. Pesquei, Fast variational Bayesian signal recovery in the presence of Poisson-Gaussian noise, in IEEE International Conference on Acoustics, Speech and Signal Processing (2016), pp.3964–3968. https://doi.org/10.1109/ICASSP.2016.7472421.

[14] J. Zhang, K. Hirakawa, and X. Jin, Quantile analysis of image sensor noise distribution, in IEEE International Conference on Acoustics, Speech and Signal Processing (2015), pp. 1598–1602. https://doi.org/10.1109/ICASSP.2015.7178240.

[15] L. Jiao, J. Zhao, A survey on the new generation of deep learning in image processing, IEEE Access 7 (2019) 172231–172263, https://doi.org/10.1109/ACCESS.2019.2956508.

[16] Y. Chen, W. Yu, T. Pock, On learning optimized reaction diffusion processes for effective image restoration, in: in *IEEE Conference on Computer Vision and Pattern Recognition* (CVPR, 2015, pp. 5261–5269, https://doi.org/10.1109/CVPR.2015.7299163.

[17] S. Lefkimmiatis, Non-local color image denoising with convolutional neural networks, in: in *IEEE Conference on Computer Vision and Pattern Recognition* (CVPR, 2017, pp. 3587–3596, https://doi.org/10.1109/CVPR.2017.623.

[18] K. Zhang, W. Zuo, Y. Chen, D. Meng, L. Zhang, Beyond a Gaussian denoiser: residual learning of Deep CNN for image denoising, IEEE Trans. Image Process. 26 (7) (2017) 3142–3155, https://doi.org/10.1109/TIP.2017.2662206.

[19] K. Zhang, W. Zuo, L. Zhang, FFDNet: Toward a fast and flexible solution for CNN based image denoising, IEEE Trans. Image Process. 27 (9) (2017) 3142–3155, https://doi.org/10.1109/TIP.2018.2839891.

[20] L. Xu, X. Tao, J. Jia, Inverse kernels for fast spatial deconvolution, in: in *Europe Conference on Computer Vision* (ECCV, 2014, pp. 33–48, https://doi.org/10.1007/978-3-319-10602-1_3.

[21] J. Sun, W. Cao, Z. Xu, J. Ponce, Learning a convolutional neural network for non-uniform motion blur removal, in: in *IEEE Conference on Computer Vision and Pattern Recognition* (CVPR, 2015, pp. 769–777, https://doi.org/10.1109/CVPR.2015.7298677.

[22] S. Nah, T.H. Kim, K.M. Lee, Deep multi-scale convolutional neural network for dynamic scene deblurring, in: In *IEEE Conference on Computer Vision and Pattern Recognition* (CVPR, 2016, pp. 257–265, https://doi.org/10.1109/CVPR.2017.35.

[23] A.G. Barto, in: Reinforcement learning, in *Neural Systems for Control*, (Academic Press, 1997, pp. 7–30.

[24] R.S. Sutton, A.G. Barto, Reinforcement learning: An introduction, MIT Press, 1998.

[25] K. Yu, C. Dong, L. Lin, C.C. Loy, Crafting a toolchain for image restoration by deep reinforcement learning, in: in *IEEE Conference on Computer Vision and Pattern Recognition* (CVPR, 2018, pp. 2443–2452, https://doi.org/10.1109/CVPR.2018.00259.

[26] M. Xie, Z. Zhang, W. Zheng, Y. Li, K. Cao, Multi-frame star image denoising algorithm based on deep reinforcement learning and mixed Poisson-Gaussian likelihood, Sensors 20 (21) (2020) 5983, https://doi.org/10.3390/s20215983.

[27] J.G. Tough, The computation of the area, centroid, and principal axes of a polygon, Comput. Geosci. 14 (5) (1988) 715–717, https://doi.org/10.1016/0098-3004(88)90025-8.

[28] G. Rufina, D. Accardo, Enhancement of the centroiding algorithm for star tracker measure refinement, Acta Astronaut. 53 (2) (2003) 135–147, https://doi.org/10.1016/S0094-5765(02)00199-6.

[29] X. Wei, J. Xu, J. Li, J. Yang, G. Zhang, S-curve centroiding error correction for star sensor, Acta Astronaut. 99 (2014) 231–241, https://doi.org/10.1016/j.actaastro.2014.03.002.

[30] M.W. Knutson, Fast star tracker centroid algorithm for high performance CubeSat with air bearing validation, Doctoral Thesis, Massachusetts Institute of Technology, Cambridge, MA, 2012.

[31] V. Mnih, K. Kavukcuoglu, D. Silver, A.A. Rusu, J. Veness, M.G. Bellemare, A. Graves, M. Riedmiller, A.K. Fidjeland, G. Ostrovski, Human-level control through deep reinforcement learning, Nature 518 (7540) (2015) 529–533, https://doi.org/10.1038/nature14236.

[32] S. Hochreiter, J. Schmidhuber, Long short-term memory, Neural Comput. 9 (8) (1997) 1735–1780, https://doi.org/10.1162/neco.1997.9.8.1735.

[33] M. Sundermeyer, H. Ney, R. Schluter, From feedforward to recurrent LSTM neural networks for language modeling, IEEE/ACM Trans. Audio Speech Lang. Process. 23 (3) (2015) 517–529, https://doi.org/10.1109/TASLP.2015.2400218.

[34] M. Abadi, P. Barham, J. Chen, Z. Chen, A. Davis, J. Dean, M. Devin, S. Ghemawat, G. Irving, M. Isard, M. Kudlur, J. Levenberg, R. Monga, S. Moore, D. G. Murray, B. Steiner, P. Tucker, V. Vasudevan, P. Warden, M. Wicke, Y. Yu, and X. Zheng, TensorFlow: A system for large-scale machine learning, In the 12th USENIX Symposium on Operating System Design and Implementation (OSDI, 2016), pp. 265–283.

[35] D. Kingma and J. Ba, Adam: A method for stochastic optimization, arXiv: 1412.6980v9 (2015).

[36] Y. Zhang, P. Song, Q. Dai, Fourier ptychographic microscopy using a generalized Anscombe transform approximation of the mixed Poisson-Gaussian likelihood, Opt. Express 25 (1) (2017) 168–179, https://doi.org/10.1364/OE.25.000168.